Reac Kinet Mech Cat
DOI 10.1007/s11144-016-1097-3

Photocatalytic degradation of phenol using doped titania supported on photonic SiO_2 spheres

Keyla M. Fuentes[1,2] · Paulino Betancourt[3] · Santiago Marrero[3] · Samuel García[4]

Received: 13 September 2016 / Accepted: 22 October 2016

Abstract The photocatalytic degradation of phenol in aqueous suspensions of co-doped TiO_2 supported on SiO_2 spheres was investigated. A novel photocatalyst was prepared combining iron doped TiO_2–SiO_2 and reduced TiO_2–SiO_2 by mechanical milling (MM/TiO_2–SiO_2). All the particles were characterized by BET. nitrogen adsorption, X-ray diffraction, scanning electron microscopy, UV–visible spectroscopy and elemental analysis. Trough XRD patterns it was calculated that 2 nm rutile crystallites were formed onto SiO_2 surface, ICP analysis confirmed Ti content near to nominal, while EDX analysis shows a surface content 10 lower, suggesting that the SiO_2 limiting the agglomeration of TiO_2 particles allowing a good dispersion. Phenol photodegradation was induced by illuminating the coated spheres in aqueous solution with a visible light source. The synthesized TiO_2–SiO_2 particles appeared to be 1.3 times more efficient in the phenol conversion, as compared to pure rutile particles. According to characterization results, this improvement could be attributed mainly to three factors: an effective transference of charge carriers trough the grain boundaries present between contact points, a photonic behavior evidenced on an increment on UV–vis absorption intensity and the quantum size effect of rutile crystallites coated on SiO_2.

✉ Keyla M. Fuentes
keylafuentesflores@gmail.com; keyla.fuentes@ucv.ve

[1] Departamento de Química Aplicada, Facultad de Ingeniería, Universidad Central de Venezuela, Caracas 40679, Venezuela

[2] INQUIMAE-DQIAQF, Facultad de Ciencias Exactas y Naturales, Universidad de Buenos Aires, Ciudad Universitaria, Pab. II, C1428EHA Buenos Aires, Argentina

[3] Laboratorio de Desarrollo de Procesos, Centro de Catálisis Petróleo y Petroquímica, Universidad Central de Venezuela, Caracas, Venezuela

[4] Centro de Microscopía Electrónica, Facultad de Ingeniería, Universidad Central de Venezuela, Caracas, Venezuela

Published online: 01 November 2016

Keywords Photonic SiO_2 spheres · Co-doped TiO_2 · Grain boundaries · Phenol degradation · Visible light

Introduction

Photocatalysis is a topic of great interest in view of its application in effluent decontamination. Among various oxide semiconductor photocatalysts, TiO_2 appears to be the most promising and important prospect for use in environmental remediation due to its strong oxidizing power, hydrophilicity, long-term stability and non-toxicity [1–3]. Several studies have been focused on its unique performance in photocatalytic degradation of toxic components, such as DDT, dichloronitrobenzene, trichlorethlyene, H_2S, NO, Cr(VI), and phenols, etc. [4–7]. Phenols are, for different purposes, widely used compounds and are present in a great variety of waste effluents of different industries, such as petrochemicals, paper mills, herbicides, fungicides, etc. [8]. These compounds are quite toxic and slowly degraded in the environment, giving different aromatic intermediates; most of them are also of environmental concern [9]. In this way, the use of semiconductor photocatalysis with TiO_2 has been proved to be a good choice to achieve a readily elimination of phenolic compounds [10].

However, technological applications of photocatalysis have some drawbacks. First, TiO_2 is not active under visible light and make use of only the 3–4% of the solar beams that reach the earth, depending on the use of an ultraviolet light source (such as a mercury lamp). Therefore, a visible light active photocatalyst becomes a requirement in order to take full advantage of solar light. This improvement will not only depend on charge carrier formation, but also on the interfacial electron transfer efficiency and rate of the electron–hole pair recombination [11]. Some modification strategies over TiO_2 particles have been proposed to achieve these goals, e.g., transition metal ion doping and/or production of oxygen deficient materials. In this regard, iron doped TiO_2 results the most studied system, relating this improvement to: (i) suppression of electron–hole recombination and (ii) lowering the band gap energy by induction of defect states inside TiO_2 gap [12–14]. On the other hand, recent studies have pointed out that the large content of oxygen vacancies (OV) present in reduced TiO_2 surfaces favors the oxidant adsorption tuning the generation of active oxygen species $O_2^{\bullet-}$ radicals and also shrinks the band-gap energy [15–17].

Another drawback arises in the light intensity decay as it passes through a photoreactor, because of absorption and scattering events by photocatalyst or other particles in the reactor. Consequently, the photon energy and the rate of photon absorption are not constant throughout the photoreactor [18]. Uniform light distribution inside the reactor is fundamental for high efficiencies; therefore to avoid energy loss by light dispersion results in another challenge to solve nowadays.

Taking these into account, an optically active system is required for leading a free propagation of energy throughout the material, such as photonics solids. Photonic materials have been extensively studied for their potential applications in optical devices due to their unique optical diffraction properties [19]. In such

structures, the dielectric constant is spatially modulated in several dimensionalities (i.e., 1D, 2D or 3D), by imposing a periodicity of the order of the light wavelength. Three dimensional self-assembled systems based on SiO_2 or latex sub-micrometric spheres have been synthesized [20, 21]. Therefore, if a semiconductor is coupled to a photonic band gap material, the spontaneous emission can be suppressed because the phonons produced during photoelectron relaxation (from the conduction band to the valence band) cannot be emitted if semiconductor bandgap matches with photonic bandgap [22]. In the last 3 years, numerous studies have proposed the effectivity of coating anatase particles in SiO_2 spheres acting as light scattering centers. The first studies were focused on dye-sensitized solar cells devices [23, 24]. Meanwhile, for photocatalytic purposes, dyes are the preferred target molecules using TiO_2 anatase phase onto SiO_2 spheres. Ubirajara et al. reported 5 nm anatase crystallites over $\sim$200 nm SiO_2 spheres for crystal violet degradation under UV light, the best results were obtained with an apparent surface coverage of 75% [25]. Ji et al. tested hollow TiO_2–SiO_2 nanospheres for methylene blue, methyl orange and phenol under natural solar light, the prepared catalyst keep its high efficiency compared with UV light experiments [26].

Considering the above mentioned, we have been tempted to assume that the contact between SiO_2 photonic structures and modified rutile TiO_2 (trough iron doping and OV generation) could be a crucial factor in the genesis of a highly active photocatalysts. The present studies were undertaken to investigate the photocatalytic performance of doped TiO_2–SiO_2 over phenol photodegradation under visible light. X-ray diffraction (XRD), specific surface area (SSA, N_2-BET), scanning electron microscopy (SEM), chemical analysis (ICP, EDX), and UV–visible absorption were used as the principal methods for catalyst characterization.

Experimental

Reagents

All the chemicals that were used in the experiments were of laboratory reagent grade and used as received without further purification. In all experiments, distilled water was used. The gases were provided by AGA gases.

Synthesis of TiO_2 reference catalyst

$TiCl_4$ (98%, Sigma-Aldrich) was slowly added dropwise into ethanol at room temperature in a molar ratio 1:100. Then sufficient acidulated water (pH 4.7) was added to obtain $Ti:H_2O = 1$. The sol–gel solution was vacuum dried at 80 °C until a solid was obtained. The solid precursor was calcined in air at 500 °C by 2 h to form TiO_2 powder (as reference catalysts). Its phase was primarily rutile with a surface area of 35 $m^2\ g^{-1}$ and crystallite size of ca. 19 nm.

Fabrication of doped TiO_2 on photonic SiO_2 sphere

SiO_2 spheres synthesis

Three-dimensional ordered SiO_2 spheres were synthesized by a sol–gel procedure following the well-known Stöber–Fink–Bohn (SFB) method [27]. This method is based on the hydrolysis of 0.266 M tetraethoxysilane (TEOS, Sigma-Aldrich) and later polymerization of Si–O–Si chains in an ethanolic medium with ammonium hydroxide (25%) as a catalyst. This sub-micrometric SiO_2 spheres ordered in a close packed arrangement has been shown to behave as photonic crystals. The as-synthesized silica powder was purified and re-dispersed in ethanol by at least three centrifugation/redispersion cycles. The obtained solid was dry at 60 °C by 2 h.

Coating SiO_2 spheres with titania nanoparticles

A solution of $TiCl_4$ in ethanol was prepared using a molar ratio of 1:100. Sufficient acidulated water (pH 4.7) was added to obtain $Ti:H_2O = 1$. This mixture was homogenized, transferred to an addition flask and dropwise added to an ethanolic suspension of the previously prepared silica spheres, (sonicated during 5 min). The Si:Ti molar ratio was fixed at nominal value of 2. The mixture was stirred for 24 h at room temperature, and then solvent was removed by vacuum extraction. parts. Finally, the solid was divided in three parts; one was calcined at 500 °C for 2 h (TiO_2–SiO_2), and the other two were used in the doping stage.

Doped and co-doped TiO_2–SiO_2 spheres

In this stage, two treatments were used: (i) doping with a $Fe(NO_3)_3$, managed to 0.05% mol Fe related to titania. The iron salt was incorporated by wetness impregnation, and the resulted solid was calcined at 500 °C for 2 h (Fe/TiO_2–SiO_2). (ii) The last portion of divided material was reduced by hydrogen (50 mL min^{-1}, 500 °C, and 2 h) (R/TiO_2–SiO_2). Finally, both solids were combined by hand milling with an agate mortar, with equivalents mass proportions, in order to obtain a co-doped photocatalyst, which acronym is MM/TiO_2–SiO_2.

Characterization

The BET surface areas of catalysts were calculated from the nitrogen adsorption isotherm at −196 °C measured in a Micromeritics ASAP 2010C apparatus. BET SSA and BJH pore volume were calculated using the software provided with this system.

Crystal phases of the solids were identified by X-ray ($\lambda = 1.792$ Å) diffraction as performed on a powder diffractometer (Bruker D-8 Advance), operating with Co K_α radiation at 40 kV and 35 mA, scanning rate of 0.02° s^{-1} in 2θ ranging from 15° to 90°. The average grain size of the TiO_2 was calculated using X-ray line broadening methods based on the Scherrer formula. The XRD phases present in the samples were identified using JCPDF Powder Data Files.

UV–visible absorption spectra of the solids suspensions in water (concentration ca. 1 g L^{-1}) were recorded at room temperature on a Jenway 6175 UV–vis spectrometer in the range from 190 to 1000 nm.

The morphology of the powder was investigated by scanning electron microscopy (SEM). A SEM sample was made by spraying a sonicated suspension of samples in ethanol onto a conductive carbon tape; the sample was sputtered with gold before imaging. The SEM image was performed on a Hitachi S2400, operated at 20 kV. EDX analysis was also performed on selected images.

ICP-OES Jobin–Yvon Ultima 2 equipment was used to quantify Ti and Fe.

Phocatalytic experimental procedure

Experiments were carried out in a 0.5 L Pyrex batch photoreactor (containing a jacketed glass tube together with water circulation to avoid overheating). The reaction mixture inside the cell was maintained in the suspension by mechanical stirring. In all experiments, air was continuously bubbled through the solution. The source of irradiation is placed outside of the reactor; it was a 150 W halogen lamp (Phillips), with an irradiance of 16 W cm^{-2} in the UV region and 28 W cm^{-2} in the visible region. The IR fraction of the incident beam was removed by the water in the double jacket of the photoreactor. The initial pH of the reaction suspension (pH $\sim$6.7) was not adjusted so it could be running freely during experiments. The analytical error of these measurements was less than 10%, it was estimated calculating the percentage error of phenol conversion for several runs done with anatase TiO_2 under almost similar reaction conditions.

Prior to photocatalytic experiments, photolysis experiments were carried out for phenol under the same experimental conditions as used for photodegradation reactions. The catalyst amount and the phenol concentrations used were 1 g L^{-1}, and 50 mg L^{-1}. The photoreactivity runs were extended along 2 h with a 15 min pre-adsorption run. Samples of 15 mL volume were withdrawn from the suspensions during reaction time and the catalysts were separated from the solution by centrifugation in each aliquot. The quantitative determination phenol was performed by chemical oxygen demand following the method 5220 D of standard methods. [28].

Results and discussion

In order to confirm the concentration of Ti and Fe, the samples were analyzed by ICP after calcination. The ICP elemental analysis results are presented in Table 1, which were in fair accordance with the nominal contents. Energy-dispersive X-ray

Table 1 Chemical analysis for MM/TiO_2 photocatalyst

	Nominal content (%p/p)		ICP analysis (%p/p)		EDX analysis (%p/p)	
	Ti	Fe	Ti	Fe	Ti	Fe
MM/TiO_2–SiO_2	46.0	1.3	43.9	0.8	5.00	0.07

analysis (EDX) has been carried out to determine the growth of titania on silica particles, and furthermore to show the distribution of elements (Fe, Ti) on the surface. EDX results showed the following: (i) Ti and Fe content is smaller than the expected value (10 times lower than nominal value), which is strongly influenced by morphological effects and heterogeneity of the sample; (ii) nanometric titania particles are assembled onto micrometer-scale SiO_2-spheres during coating process.

The SiO_2-spheres shows no hysteresis loops (type II adsorption isotherms according to Brunauer classification). However, the TiO_2 and MM/TiO_2–SiO_2 samples show small hysteresis loops at higher relative pressure implying the presence of mesoporosity. The SiO_2-spheres has a narrow pore size distribution with an average pore diameter around 3 nm and SSA of 14 $m^2\ g^{-1}$. When TiO_2 was supported on a SiO_2, including Fe incorporation and thermal treatments, the SSA of MM/TiO_2–SiO_2 was close to SiO_2. The SSA, total pore volume, and average pore diameter of MM/TiO_2–SiO_2 solid are 17 $m^2\ g^{-1}$, 0.33 $cm^{-3}\ g^{-1}$, and 20 nm. The surface area mainly comes from its cover material, which consists of titania crystalline particles formed in the self-assembly process.

The crystal structure of the SiO_2, TiO_2–SiO_2, MM/TiO_2–SiO_2, and TiO_2 solids samples were examined by XRD (Fig. 1). The experimental peak positions were compared with the standard JCPDS files and the corresponding Miller indices were established. Fig. 1a shows an X-ray powder diffraction pattern of precipitated SiO_2. An amorphous peak with the equivalent Bragg angle at $2\theta = 23°$ was recorded (JCPDS 29-0085). Martinez et al. [29] prepared amorphous SiO_2 by the sol–gel procedure, subjected it to thermal treatment, and then analyzed it using the Rietveld refinement. In their work, an amorphous peak was centered at $2\theta = 23°$. Furthermore, Zhang et al. [30] also recorded one broadened XRD peak for amorphous silica centered at a 2θ value close to our measurement. This feature would explain the spherical morphology and low surface area values, because there

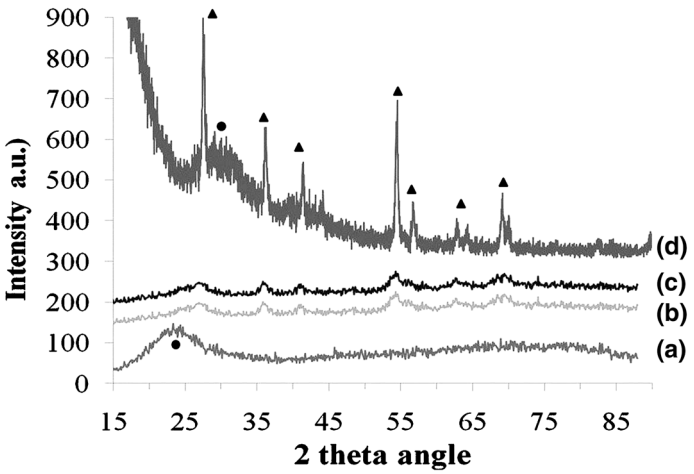

Fig. 1 XRD patterns of the prepared solids (*a*) SiO_2 spheres, (*b*) calcined TiO_2–SiO_2, (*c*) MM/TiO_2–SiO_2, (*d*) pure TiO_2. *Circle* represents [101] index for amorphous silica according JCPDF 77-1315, *triangles* represents index for rutile TiO_2 according JCPD 86-2485

are no preferential directions for crystal growth. Supporting it, Shen et al. [31] have prepared monodisperse spherical SiO_2 and they have reported that the as-prepared SiO_2 particles were amorphous with no crystallized phases.

The XRD measurements revealed that the samples showed a clear rutile-type crystal structure (JCPDF 86-0147) and no evidence of anatase (see Figs. 1b–1d). It has been reported by Chen et al. that increasing the acidity in the reaction medium and the concentration of $TiC1_4$ aqueous solution favored the formation of rutile phase [32]. In the present study, all of the solids were prepared using $TiC1_4$ and the diffractograms reveal that all of the samples possess a rutile phase.

From the crystallite size data in Table 2, it appears that the SiO_2 sphere has an effect on the crystallite size of rutile, the presence of SiO_2 results in smaller crystallite size. This effect may be due to the SiO_2 limiting the agglomeration of TiO_2 particles. The morphology of the silica and titania particles were examined using SEM. Fig. 2 shows the SEM images of TiO_2 covered on SiO_2 spheres. This result confirms the spherical morphology of particles. The mean diameter of SiO_2 spheres is about 195 nm with little dispersion in size distribution (Fig. 2a). Then, the solid covered with TiO_2 nanoparticles before thermal treatments (Fig. 2b) shows the same morphology, and almost any change in the average particle size of the spheres. While, the image corresponding to the MM/TiO_2–SiO_2 photocatalyst (Fig. 2c) reveals that some particles became agglomerated leading to higher defect/grain boundary concentration.

Fig. 3 shows the absorption spectra of the prepared samples dispersed in water. These results highlight the strongest absorption at around 300 nm for the combined solids (co-doped and undoped) in comparison to pure TiO_2 and SiO_2. A clear red shift in the absorption edges of solids is seen in Fig. 3. These improvements are illustrated in the better dispersion of the photocatalyst in water (evidenced in the higher absorption intensity) and a better visible light absorption (showed in the band shift to lower energy values). Moreover, the results show a great potential of this material for solar photocatalysis applications. The band-gap energies for the samples were calculated from the straight part of the optical absorption spectra [33]. The presence of iron-oxo centers and oxygen vacancies on the surface of TiO_2–SiO_2 shifts the bandgap from 3.53 eV for rutile to 3.24 eV, differences with reported value of 3.0 eV can be attributed to the dependence of the band gap with the particle size and light scattering phenomena [34]. Below a certain threshold, the density of point/surface defects of semiconductor crystalline increases with decrease in particle size. This red shift in the absorption spectrum is caused by strengthening of the quantum confinement of charge carriers at a decrease in the size of TiO_2 nanocrystalline particles according to the observed in XRD patterns. Zribi et al. obtained similar evolution of optical band gap and concluded that the variation of

Table 2 Rutile crystallite size for the obtained solids

Solid	Rutile crystallite size (nm)
TiO_2	19
TiO–SiO_2	2
MM/TiO_2–SiO_2	2

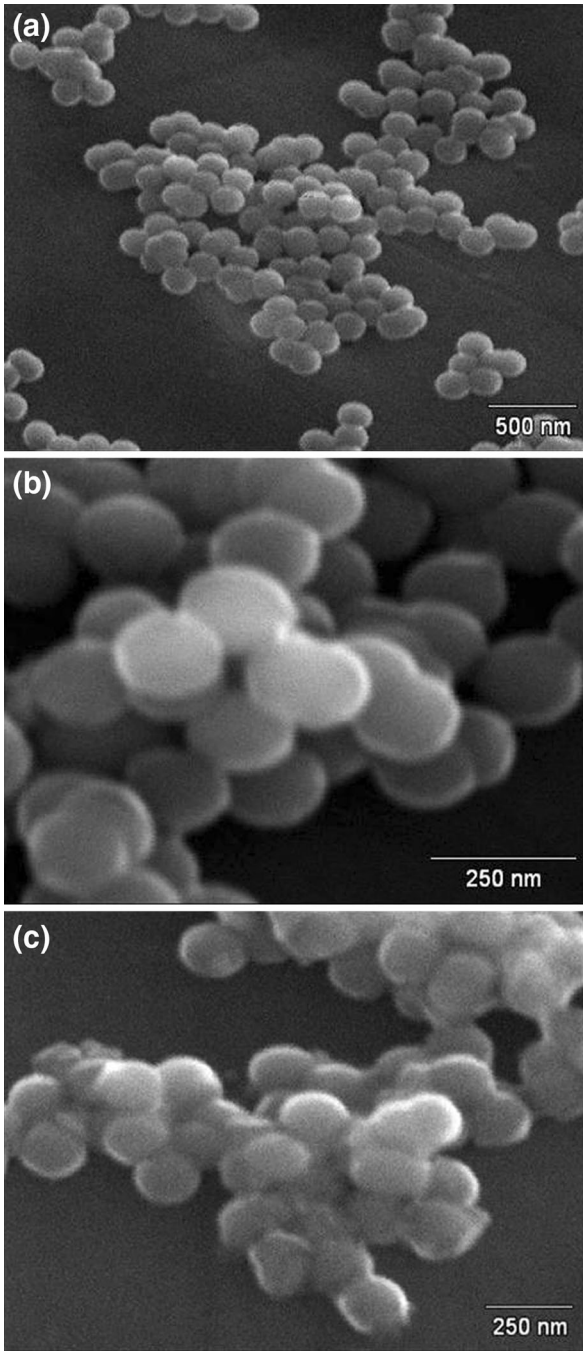

Fig. 2 MEB micrographs **a** SiO_2 spheres (magnification 15 K), **b** un-calcined TiO_2–SiO_2 (magnification 30 K), **c** MM/TiO_2–SiO_2 phtocatalyst (magnification 30 K). Acceleration voltage in all runs was 20 kV

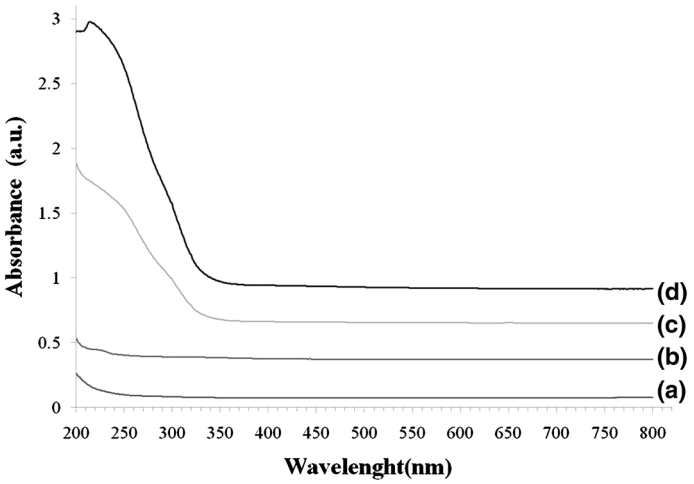

Fig. 3 UV–vis absorption spectra of the prepared solids in aqueous suspensions. Each solid suspension of 1 g L^{-1} were sonicated 5 min and immediately measured. (*a*) Pure TiO_2, (*b*) SiO_2 spheres, (*c*) calcined TiO_2–SiO_2, (*d*) MM/TiO_2–SiO_2

the structural modifications may be responsible for changes in the shape of the fundamental absorption edge [35]. A good photocatalyst must have high photon conversion efficiency. In fact, the particle size of photocatalysts determines the photon conversion efficiency.

Stroyuk has explained that several processes must be taking into account when photocatalyst crystal size diminishes, such as the rapid diffusion of the photogenerated charges to the surface of the nanocrystal. The increase of E_g caused by the structurally imperfect surface of the nanoparticles, causing an increase in the potentials of the photogenerated charges, and the ability of the nanostructured semiconductors to accumulate high densities of charge, etc. All these processes favor the effective transformation of light quanta into chemically active particles (electrons and holes) and also the charges transfer to donor and acceptor substrates [36].

Finally, we have tested pure rutile-TiO_2, TiO_2/SiO_2 and MM/TiO_2/SiO_2 toward photodegradation of phenol under visible light in order to confirm their novel photochemical properties, Fig. 4 reveals this behavior. The photolysis experiments shows a conversion of 12% under the experimental conditions. Comparing all doped catalyst respect to pure TiO_2, clearly a higher performance is observed, indicating that combination of rutile phase with SiO_2 spheres drastically improves its photocatalytic activity. Several authors have reported an enhancement of TiO_2 photoactivity when it is combined with SiO_2 [26, 37–39]. In the photocatalysts studied in this paper, appear to be several processes operating simultaneously: the quantum size effect, photonic behavior, and defects/grain boundaries. SiO_2 interaction with TiO_2 would facilitate the quantum size effect due to limitations of TiO_2 crystal growth, exhibiting peculiar electronic properties [40]. Additionally, it has been reported that in TiO_2 coated SiO_2, the SiO_2 core acts as light dispersion

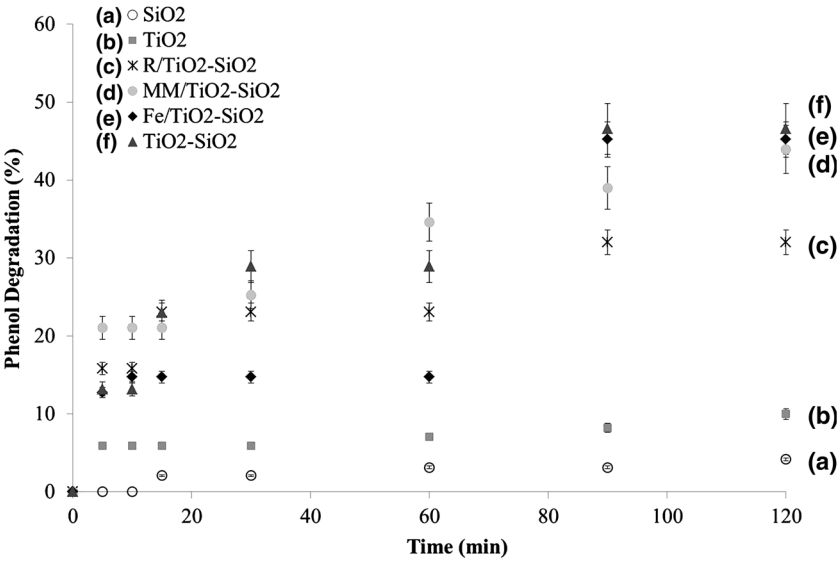

Fig. 4 Percentage of phenol degradation versus reaction time using the prepared photocatalysts: (*a*) SiO_2, (*b*) pure TiO_2, (*c*) R/TiO_2–SiO_2, (*d*) MM/TiO_2–SiO_2, (*e*) Fe/TiO_2–SiO_2, (*f*) TiO_2–SiO_2. Experimental conditions: [phenol] = 50 mg L^{-1}, [catalyst] = 1 g L^{-1}, temperature = 25 °C, volume = 0.25 L, light source = 150 W halogen lamp 16 mw cm^{-2} in UV region, O_2 flow = 1 L min^{-1}

center and hence increasing TiO_2 photoactivity [41]. Such processes of dispersion and reflection of light are able to guarantee a higher value of the quantum yield (photonic solid behavior). Ultimately, in our case, TiO_2 nanoparticles covers SiO_2 spheres, which cause contact points by agglomeration induced during the thermal treatment. At this point, we could propose that charge transport in this contact points (grain boundaries) enhances phenol photocatalytic degradation. It has been reported that the photoinduced charge transfer mechanism is different in isolated particles compared to agglomerated nanoparticles. In the last case, an energetic interconnection favors the photogenerated charge separation [42]. Sheppard et al. carried out comparative studies over mono and poly-TiO_2 crystals, as well over an anatase–rutile mixture; they concluded that defects points as oxygen vacancies or grain boundaries acts like electronic donors [43, 44]. The results obtained indicate that in these regions, weak ionic bonds are formed, allowing the charge transport throughout the material. In summary, grain boundaries do not act as charge recombination centers, differing to others authors [45]. It has been proposed that nanoparticles forms agglomerates connected through grain boundaries, supporting the existence of an "antenna mechanism". The so-called "antenna mechanism" the resulting energetic coupling throughout a long chain of titania nanoparticles will enable an energy transfer from the particle where the initial photon absorption took place to the particle where the electron transfer process finally occurs [42, 46].

The comparison of photoactivity for TiO_2–SiO_2 materials respect to unsupported rutile are displayed in Fig. 5, activity (a) was calculated as the ratio between

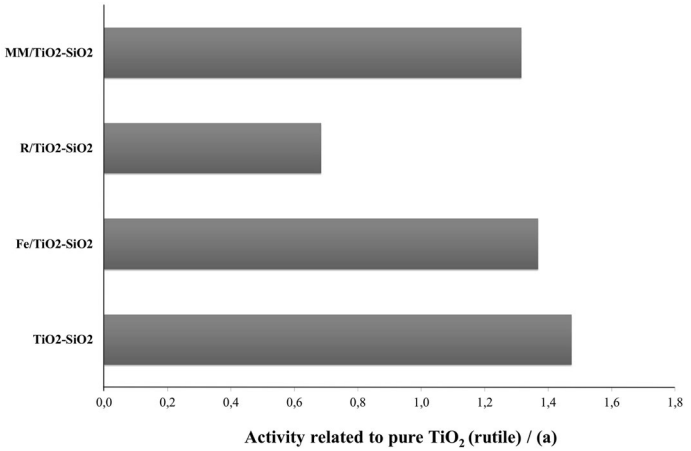

Fig. 5 Photoactivity of the prepared photocataslyst related to pure rutile. Activity was calculated as the ratio between the conversion improvements related to rutile and pure rutile conversion. $a = [\text{pd(cat.)} - \text{pd(rutile)}]/\text{pd(rutile)}$ with pd = percentage of phenol degradation

conversion improvements (related to rutile) and pure rutile conversion. Apparently, doping did not cause noteworthy changes in final degradation compared with the TiO_2–SiO_2 system, but photoactivity remains near 1.5 times higher than undoped rutile. However, comparing the conversion behavior represented in Fig. 4 for the co-doped material, phenol degradation at initial times is slightly higher and conversion at final reaction time (120 min) did not reach steady-state unlike the rest of the photocatalyst tested; suggesting photoactivity for MM/TiO_2–SiO_2 material could be even higher in an extended period of time.

Conclusions

The Stober-Fink-Bhon method leads the attainment of SiO_2 sphere with a homogeneous dispersion in particle size. The coating with rutile nanoparticles and subsequent co-doping, yield a novel photocatalyst with spherical morphology and high potential to act as a photonic crystal. A strong absorption as well a red-shift in Uv–vis spectra was observed in this solid, this feature allowed an important increment in photoactivity for phenol degradation under visible light. This improvement is addressed mainly to three factors: an effective transference of charge carriers trough grain boundaries existent between spheres, photonic behavior and the quantum size effect.

Acknowledgements Authors want to thanks to Consejo de Desarrollo Científico y Humanístico of Universidad Central de Venezuela for financial support through Project No. CDCH 03-8788-2013-1 and to The National Research Council of Argentina (CONICET) for the post-doctoral fellowship (2016-2018) of Dr. Fuentes. Funding was provided by Fondo para la Investigación Científica y Tecnológica (Grant No. 2282016000093200).

References

1. Schneider J, Matsuoka M, Takeuchi M, Zhang J, Horiuchi Y, Anpo M, Bahnemann D (2004) Understanding TiO_2 photocatalysis: mechanisms and materials. Chem Rev 114:9919–9986
2. Nakata K, Fujishima A (2012) TiO_2 photocatalysis: design and applications. J Photochem Photobiol C 13:169–189
3. Gaya U, Abdullah A (2008) Heterogeneous photocatalytic degradation of organic contaminants over titanium dioxide: a review of fundamentals, progress and problems. J Photochem Photobiol C 9:1–12
4. Quan X, Zhao X, Chen S, Zhao H, Chen J, Zhao Y (2005) Enhancement of *p,p′*-DDT photodegradation on soil surfaces using TiO_2 induced by UV-light. Chemosphere 60:266–273
5. Lin L, Chai C, Zhao B, Wei W, He D, He B, Tang Q (2013) Photocatalytic oxidation for degradation of VOC's. OJIC 3:14–25
6. Yuan Y, Zhang J, Li H, Li Y, Zhao Y, Zheng C (2012) Simultaneous removal of SO_2, NO and mercury using TiO_2-aluminum silicate fiber by photocatalysis. Chem Eng J 192:21–28
7. Xu S, Pan S, Xu Y, Luo Y, Zhang Y, Li G (2015) Efficient removal of Cr(VI) from wastewater under sunlight by Fe(II)-doped TiO_2 spherical shell. J Hazard Mater 11:7–13
8. Rappoport Z (2003) The chemistry of phenols. Wiley, New Jersey
9. Schwarzenbach R, Gschwend P, Imboden D (1993) Environmental organic chemistry. Wiley, New Jersey
10. Priya S, Premalatha M, Anantharaman N (2008) Solar photocatalytic treatment of phenolic wastewater-potential, challenges and opportunities. ARPN-JEAS 3:36–41
11. Green J, Carter E, Murphy D (2009) Interaction of molecular oxygen with oxygen vacancies on reduced TiO_2: site specific blocking by probe molecules. Chem Phys Lett 477:340–344
12. Castro C, Centeno A, Giraldo S (2010) Fe-modified TiO_2 photocatalysts for the oxidative degradation of recalcitrant water contaminants. Catal Today 157:119–124
13. Qamar M, Merzougui B, Anjum D, Hakeem A, Yamani Z, Bahnemann D (2014) Synthesis and photocatalytic activity of mesoporous nanocrystalline Fe-doped titanium dioxide. Catal Today 230:158–165
14. Lee T, Ryu H, Lee W (2015) Photoelectrochemical properties of iron (III)-doped TiO_2. Ceram Int 41:7582–7589
15. Wendt S, Sprunger P, Lira E, Madsen G, Li Z, Hansen J, Matthiesen J, Blekinge-Rasmussen A, Lægsgaard E, Hammer B, Besenbacher F (2008) The role of interstitial sites in the Ti3d defect state in the band gap of titania. Science 320:1755–1759
16. Zhang Z, Long J, Xie X, Zhuang H, Zhou Y, Lin H, Yuan H, Dai W, Ding Z, Wang X, Fu X (2012) A controlling the synergistic effect of oxygen vacancies and N dopants to enhance photocatalytic activity of N-doped TiO_2 by H_2 reduction. Appl Catal A 425:117–124
17. Kang Q, Cao J, Zhang Y, Liu L, Xu H, Ye J (2013) Reduced TiO_2 nanotube arrays for photoelectrochemical water splitting. J Mater Chem 1:5766–5774
18. Motegh M, Cen J, Appel P, Van Ommen J, Kreutzer M (2012) Photocatalytic-reactor efficiencies and simplified expressions to assess their relevance in kinetic experiments. Chem Eng J 207:607–615
19. Joannopoulos J, Meade R, Winn J (1995) Photonic crystals: molding the flow of light. Princeton University, New Jersey
20. Du X, He J (2013) Spherical silica micro/nanomaterials with hierarchical structures: synthesis and applications. Nanoscale 3:3984–4002
21. Jiang Q, Li K, Wei H, Yi L (2013) Tunable optical stop band of silica shell photonic crystals. J Sol–Gel Sci Techn 67:565–572
22. Meseguer F, Blanco A, Míguez H, García-Santamaría F, Ibisate M, López C (2002) Synthesis of inverse opals. Colloids Surf A 202:281–290
23. Wang Y, Chen E, Lai H, Lu B, Hu Z, Qin X, Shi W, Du G (2013) Enhanced light scattering and photovoltaic performance for dye-sensitized solar cells by embedding submicron SiO_2/TiO_2 core/shell particles in photoanode. Ceram Int 39:5407–5413
24. Son S, Hwang S, Kim C, Yun J, Jang J (2013) Designed synthesis of SiO_2/TiO_2 core/shell structure as light scattering material for highly efficient dye-sensitized solar cells. ACS Appl Mater Interfaces 5:4815–4820
25. Ullah S, Ferreira-Neto E, Pasa A, Alcântara C, Acuña J, Bilmes SA, Ricci MM, Landers R, Fermino T, Rodrigues-Filho U (2015) Enhanced photocatalytic properties of core@shell $SiO_2@TiO_2$ nanoparticles. Appl Catal B 179:333–343

26. Guo N, Liang Y, Lan S, Liu L, Ji G, Gan S, Zou H, Xu X (2014) Uniform TiO_2–SiO_2 hollow nanospheres: synthesis, characterization and enhanced adsorption–photodegradation of azo dyes and phenol. Appl Surf Sci 305:562–574
27. Stöber W, Fink A, Bohn E (1968) Controlled growth of monodisperse silica spheres in the micron size range. J Colloid Interface Sci 26:62–69
28. American Society for Testing and Materials (1995) Standard test methods for chemical oxygen demand (dichromate oxygen demand) of water. D1252-95, ASTM Annual Book of Standards. American Society of Testing and Materials, Philadelphia
29. Martínez J, Palomares S, Ortega-Zarzosa G, Ruiz F, Chumakov Y (2006) Rietveld refinement of amorphous SiO_2 prepared via sol–gel method. Mater Lett 60:3526–3529
30. Zhang G, Xu Y, Xu D, Wang D, Xue Y, Su W (2008) Pressure-induced crystallization of amorphous SiO_2 with silicon–hydroxy group and the quick synthesis of coesite under lower temperature. High Press Res 28:641–650
31. Shen X, Zhai Y, Sun Y, Gu H (2010) Preparation of monodisperse spherical SiO_2 by microwave hydrothermal method and kinetics of dehydrated hydroxyl. J Mater Technol 26:711–714
32. Cheng H, Ma J, Zhao Z, Qi L (1995) Hydrothermal preparation of uniform nanosize rutile and anatase particles. Chem Mater 7:663–671
33. Kamalasanan M, Chandra S (1996) Sol–gel synthesis of ZnO thin films. Thin Solid Films 288:112–118
34. Brus L (1986) Electronic wave functions in semiconductor clusters: experiment and theory. J Phys Chem 90:2555–2560
35. Zribi M, Kanzari M, Rezig B (2008) Structural, morphological and optical properties of thermal annealed TiO thin films. Thin Solid Films 516:1476–1482
36. Stroyuk AL, Kryukov AI, Kumchii A, Pokhodenko VD (2005) Quantum size effects in semiconductor photocatalysis. Theor Exp Chem 41:207–228
37. Anderson C, Bard A (1995) An improved photocatalyst of TiO_2/SiO_2 prepared by a sol–gel synthesis. J Phys Chem 99:9882–9885
38. Mahyar A, Behnajady M, Modirshahla N (2010) Characterization and photocatalytic activity of SiO_2–TiO_2 mixed oxide nanoparticles prepared by sol–gel method. Indian J Chem A 49:1593–1600
39. Milchi A, Janitabar S, Rasouli S (2011) Sol–gel preparation of nanoscale TiO_2/SiO_2 composite for eliminating of con red azo dye. Mater Sci Appl 2:476–480
40. Tallarida M, Das C, Schmeisser D (2014) Quantum size effects in TiO_2 thin films grown by atomic layer deposition. Beilstein J Nanotechnol 5:77–82
41. Bo Yoo J, Yoo HJ, Lim BW, Lee KH, Kim MH, Kang D, Kang D, Hur NH (2012) Controlled synthesis of monodisperse SiO_2–TiO_2 microspheres with a yolk-shell structure as effective photocatalysts. ChemSusChem 5:2334–2340
42. Park Y, Kim W, Monllor-Satoca D, Tachikawa T, Majima T, Choi W (2013) Role of interparticle charge transfers in agglomerated photocatalyst nanoparticles: demonstration in aqueous suspension of dye-sensitized TiO_2. J Phys Chem Lett 4:189–194
43. Nowotny J, Bak T, Burg T, Nowotny NK, Sheppard LR (2007) Effect of grain boundaries on semiconducting properties of TiO_2 at elevated temperatures. J Phys Chem C 111:9769–9778
44. Bak T, Nowotny J, Nowotny MK, Sheppard LR (2007) Defect chemistry of titanium dioxide effect of interfaces. J Aust Ceram Soc 43:49–55
45. Nakade S, Saito Y, Kubo W, Kitamura T, Wada Y, Yanagida S (2003) Influence of TiO_2 nanoparticle size on electron diffusion and recombination in dye-sensitized TiO_2 solar cells. J Phys Chem B 107:8607–8611
46. Wang C, Pagel R, Dohrmann J, Bahnemann D (2006) Antenna mechanism and deaggregation concept: novel mechanistic principles for photocatalysis. C R Chem 9:761–773